# Large Eddy Simulations of Two-Phase Turbulent Flows*

**S. Pannala† and S. Menon‡**
School of Aerospace Engineering
Georgia Institute of Technology
Atlanta, GA 30332-0150

## ABSTRACT

A two-phase subgrid combustion model has been developed for large-eddy simulations (LES). This approach includes a more fundamental treatment of the effects of the final stages of droplet vaporization, molecular diffusion, chemical reactions and small scale turbulent mixing than other LES closure techniques. As a result, Reynolds, Schmidt and Damkohler number effects are explicitly included. This model has been implemented within an Eulerian-Lagrangian two-phase formulation. In this approach, the liquid droplets are tracked using the Lagrangian approach up to a pre-specified cut-off size. The evaporation of the droplets larger than the cut-off size and the evaporation and mixing of droplets smaller than the cut-off size are modeled within the subgrid using an Eulerian two-phase model. It is shown that droplets with order unity Stokes number disperse more than small droplets in agreement with earlier numerical and experimental studies. Conventional and the present approach agree very well when droplets do not fall below the cut-off. However, the present approach gives consistently better results when the cut-off is increased, thereby, demonstrating an important advantage of the new method. The limitations of the current methodology are also highlighted and possible solutions are discussed.

## INTRODUCTION

Combustion efficiency, reduced emissions and stable combustion in the lean limit are some of the desirable features in the next generation gas turbine engines. To achieve these capabilities, current research is focusing on improving the liquid fuel atomization process and to increase fuel-air mixing downstream of the fuel injector. However, the structure of complex three-dimensional, fuel-air mixing layers is very difficult to resolve using current experimental and numerical methods. Since, fuel atomization and fuel-air mixing are both highly unsteady, conventional steady state methods cannot be used to elucidate the finer details. On the other hand, although the unsteady mixing process can be studied quite accurately using direct numerical simulation (DNS) (e.g., Poinsot, 1996), the application of DNS is limited to low to moderate Reynolds numbers (Re) due to resolution requirements and therefore, cannot be used for high Re flows of current interest.

In LES, the scales larger than the grid are computed using a time- and space-accurate scheme, while the unresolved smaller scales are modeled. Closure of momentum and energy transport equations can be achieved using a subgrid eddy viscosity model since the small scales primarily provide a dissipative mechanism for the energy transferred from the large scales. However, for combustion to occur, the species must first undergo mixing and come into molecular contact. These processes occur at the small scales which are not resolved in the conventional LES approach. As a result, conventional subgrid eddy diffusivity models cannot be used to model these features.

To address these issues, recently (Menon et al., 1993; Menon and Calhoon, 1996; Calhoon and Menon, 1996, 1997) a subgrid combustion model was developed and implemented within the LES formulation. This model separately and simultaneously treats the physical processes of molecular diffusion and small scale turbulent convective stirring. This is in contrast to probability density function closure which phenomenologically treats these two processes by a single model, thereby removing experimentally observed Schmidt number variations of the flow.

---

†. GRA, Student Member, AIAA
‡. Professor, Senior Member, AIAA

The gas-phase methodology was recently extended to two-phase flows (Menon and Pannala, 1997) to accurately capture the process of phase change and turbulent mixing. In the present paper, this approach has been further refined and used to study vaporization and the subsequent chemical reactions. Both infinite and finite-rate kinetics have been investigated and discussed in this paper.

## FORMULATION

Both Eulerian and Lagrangian formulations have been used to simulate two-phase flows in the past (e.g., Mostafa and Mongia, 1983). However, most state-of-the-art codes employ the Lagrangian form to capture the droplet dynamics, while the gas phase is computed in the Eulerian form (e.g., Oefelein and Yang, 1996). In this formulation, the droplets are tracked explicitly using Lagrangian equations of motion, and heat and mass transfer are computed for each droplet. Due to resource constraints (computer time and memory), only a limited range of droplet sizes are computed. Droplets below an *ad hoc* cut-off size are assumed to vaporize instantaneously and to become fully mixed in the gas phase. This is a flawed assumption, since even in pure gas flows small-scale mixing process is very important for quantitative predictions (Menon and Calhoon, 1996). Here, the gas-phase subgrid combustion methodology has been extended to allow proper simulation of the final stages of droplet evaporation and turbulent mixing.

The two-phase subgrid process is implemented within the framework of the Eulerian-Lagrangian LES approach. Thus, droplets larger than the cut-off size are tracked as in the usual Lagrangian approach. However, once the droplets are smaller than the cut-off, a two-phase subgrid Eulerian model is employed to include the effects of the small droplets within the LES cells.

### Gas Phase LES Equations

The incompressible Navier Stokes equations in the zero Mach number limit are employed for the present study. Zero-Mach number approach involves using a series expansion in terms of Mach number to remove the acoustic component from the equations and is a well established method (McMurtry et al., 1989; Chakravarthy and Menon, 1997).

The LES mass, momentum, energy and species equations in the zero-Mach number limit are:

$$\frac{\partial \rho}{\partial t} + \frac{\partial \rho \bar{u}_i}{\partial x_i} = \dot{\rho}_s \qquad (1)$$

$$\frac{\partial \rho \bar{u}_i}{\partial t} + \bar{u}_j \frac{\partial \rho \bar{u}_i}{\partial x_j} = \frac{\partial \bar{p}}{\partial x_i} + \mu \frac{\partial^2 \bar{u}_i}{\partial x_k \delta x_k} + \frac{\partial \tau_{ij}}{\partial x_j} + \dot{F}_{s,i} \qquad (2)$$

$$\frac{\partial \bar{u}_i}{\partial x_i} = \frac{\Upsilon - 1}{\Upsilon} \frac{1}{\hat{p}} \left[ \lambda \frac{\partial^2 T}{\partial x_k \partial x_k} - \frac{\Upsilon}{\Upsilon - 1} \frac{\partial \hat{p}}{\partial t} + \dot{Q}_s - \dot{F}_{s,i} + \dot{\rho}_s ((u_i u_i)/2) \right] \qquad (3)$$

$$\frac{\partial \rho \overline{Y_\alpha}}{\partial t} + \frac{\partial \rho \overline{Y_\alpha} u_j}{\partial x_j} = D \frac{\partial^2 \overline{Y_\alpha}}{\partial x_k \partial x_k} + \frac{\partial S_{\alpha j}}{\partial x_j} + \overline{\dot{\omega}_\alpha} + S_{s,\alpha} \qquad (4)$$

The above system of equations is supplemented by the equation of state for the thermodynamic pressure $\hat{p} = \rho RT$ which can be used to obtain the temperature $T$. Here, $\rho, \bar{u}_i, \overline{Y_\alpha}$ and $\bar{p}$ are, respectively, the density, i-th velocity component, $\alpha$-th species mass fraction and the kinematic pressure. Also, $\nu, \lambda, D$ and R are, respectively, the kinematic viscosity, the thermal conductivity, the mass diffusion (assumed constant and same for all species here, but can be generalized) and the gas constant. In Eq. (4), $\overline{\dot{\omega}_\alpha}$ is the LES filtered species production/destruction term. Also, in the above equations, source terms $\dot{\rho}_s, \dot{F}_s, \dot{Q}_s$, and $S_s$ represent the volume-averaged rate of exchange of mass, momentum, energy and species between the gas-phase and the liquid phase. These terms are computed, as detailed elsewhere (Oefelein and Yang, 1996; Faeth, 1983) and, therefore, omitted here for brevity. Furthermore, note that Eq. (3) is the equivalent energy equation in the zero-Mach number limit. In the absence of heat release and no phase change, this equation and Eq. (1) will be identical.

In the above equations, the subgrid stress tensor $\tau_{ij} = -(\overline{u_i u_j} - \bar{u}_i \bar{u}_j)$ and the species-velocity correlations $S_{\alpha j} = -(\overline{Y_\alpha u_j} - \overline{Y_\alpha} \bar{u}_j)$ require modeling. In the present LES approach, the stress term $\tau_{ij}$ is modeled as $\tau_{ij} = 2\nu_t S_{ij}$ where $\nu_t$ is the eddy viscosity and $S_{ij}$ is the resolved rate-of-strain tensor. The subgrid eddy viscosity is obtained in terms of the grid scale $\Delta$ and the subgrid kinetic energy, $k_s = (\overline{u_i u_i} - \bar{u}_i \bar{u}_i)$ as: $\nu_t = C_\nu \sqrt{k_s} \Delta$. Here, $k_s$ is obtained by solving a transport equation (e.g., Menon and Kim, 1996). The coefficient $C_\nu$ in the eddy viscosity model and the coefficients appearing in the $k_s$ equation can be obtained using the dynamic

procedure as described elsewhere (Menon and Kim, 1996).

**Liquid-phase LES equations**

A Stochastic Separated Flow (SSF) formulation (Faeth, 1983; Oefelein and Yang, 1996) is used to track the droplets using Lagrangian equations of motion. The general equations of spherical droplets reduce to the following form (here, terms arising due to static pressure gradient, virtual-mass, Besset force and external body-forces are neglected for simplicity):

$$\frac{dx_{p,i}}{dt} = u_i \tag{5}$$

$$\frac{du_{p,i}}{dt} = \frac{3}{4} C_D Re_p \frac{\mu}{\rho_p d_p^2}(u_i - u_{p,i}) \tag{6}$$

where the droplet properties are denoted by subscript p, $d_p$ is the droplet diameter and $u_i$ is the instantaneous gas phase velocities computed at the droplet location. This gas phase velocity field is obtained using both the filtered LES velocity field $\bar{u}_i$ and the subgrid kinetic energy $k^{sgs}$ (as in the eddy interaction model). The droplet Reynolds number is computed using: $Re_p = \frac{d_p}{\nu}[(u_i - u_{p,i})(u_i - u_{p,i})]^{1/2}$ and the drag coefficient is modeled by (Faeth, 1983):

$$C_D = \begin{cases} \frac{24}{Re_p}\left(1 + \frac{1}{6}Re_p\right) & Re_p \le 10^3 \\ 0.424 & Re_p > 10^3 \end{cases} \tag{7}$$

The conservation of the mass of the droplets results is given by: $d\dot{m}_p/dt = -\dot{m}_p$ where the mass transfer rate for a droplet in a convective flow field is given as:

$$\frac{\dot{m}_p}{\dot{m}_{Re_p=0}} = 1 + \frac{0.278 Re_p^{1/2} Sc^{1/3}}{[1 + 1.232/Re_p Sc^{2/3}]^{1/2}} \tag{8}$$

Here, Sc is the Schmidt number and the subscript $Re_p = 0$ indicates quiescent atmosphere when there is no velocity difference between the gas and the liquid phase. The mass transfer under this condition is given as $\dot{m}_{Re_p=0} = 2\pi\rho_s D_{sm} d_p ln(1 + B_M)$ . Here, $\rho_s$ and $D_{sm}$ are, respectively, the gas mixture density and the mixture diffusion coefficient at the droplet surface and $B_M$ is the Spalding number which is given as $B_M = (Y_{s,F} - Y_{\infty,F})/(1 - Y_{s,F})$ . Here, $Y_{s,F}$ is the fuel mass fraction at the surface of the droplet and computed using the procedure described in Chen and Shuen (1993), while $Y_{\infty,F}$ is the fuel mass fraction in the ambient gas.

The heat transfer rate of the droplet (assuming uniform temperature in the droplet) is given by the following relation (Faeth, 1983):

$$m_p C_{p,p} \frac{dT_p}{dt} = h_p \pi d_p^2 (T - T_p) - \dot{m}_p \Delta h_v \tag{9}$$

The heat transfer coefficient for a droplet in a convective flow field with mass transfer is modeled as

$$\frac{h_p}{h_{Re_p=0}} = 1 + \frac{0.278 Re_p^{1/2} Pr^{1/3}}{[1 + 1.232/Re_p Pr^{2/3}]^{1/2}} \tag{10}$$

Here, Pr is the gas phase Prandtl number and the heat transfer coefficient for quiescent medium is given as $h_{Re_p=0} = \lambda Nu_{Re_p=0}/d_p$ where the Nusselt number is obtained from:

$$Nu_{Re_p=0} = \frac{2 ln(1 + B_M)^{Le^{-1}}}{(1 + B_M)^{Le^{-1}} - 1} \tag{11}$$

$Nu_{Re_p=0}$ approaches a value of 2 in the case of zero mass transfer and Le is the Lewis number. Only droplets above a cut-off diameter are solved using the above equations, while the droplets below the cut-off diameter are modeled using Eulerian formulation within the subgrid.

In summary, the present LES approach solves only the momentum equations on the LES grid. Closure for the subgrid stresses is achieved by using a localized dynamic model for the subgrid kinetic energy. Concurrently, the liquid phase equations are solved using the Lagrangian technique. The range of droplet sizes tracked depends on the computational constraints. The gas phase LES velocity field and the subgrid kinetic energy are used to estimate the instantaneous gas velocity at the droplet location. This essentially provides a coupling between the gas and liquid phase momentum transport. The mass conservation and the

gas phase scalar field equations are simulated in the subgrid domain as discussed in the next section.

## SUBGRID COMBUSTION MODELS

The principle difficulty in reacting LES simulations is the proper modeling of the combustion related terms involving temperature and species, for example, the convective species fluxes such as $S_{\alpha j}$ due to subgrid fluctuations and the filtered species mass production rate $\dot{\omega}_\alpha$. Probability density function methods when applied within LES either using assumed shape or evolution equation may be used to close $\dot{\omega}_\alpha$ and, in principle, any scalar correlations. However, the treatment of molecular mixing and small scale stirring using phenomenological models as in pdf methods, have not been very successful in predicting the mixing effects. Problems have also been noted when the gradient diffusion model is used to approximate the species transport terms.

The linear eddy mixing (LEM) model treats separately molecular diffusion and turbulent mixing processes at all relevant length scales of the flow. The scalar fields are simulated within a 1D domain which, in the context of LES, represents a 1D slice of the subgrid flame brush. The subgrid model simulates only the effect of the small unresolved scales on the scalar fields while the larger resolved turbulent scales of the flow are simulated by the LES equations. The subgrid LEM has several advantages over conventional LES of reacting flows. In addition to providing an accurate treatment of the small-scale turbulent mixing and molecular diffusion processes, this method avoids gradient diffusion modeling of scalar transport. Thus, both co- and counter-gradient diffusion can be simulated. More details of this approach (which is identical to the method used for gas phase LES) is given elsewhere (Menon and Calhoon, 1996; Calhoon and Menon, 1996, 1997) and therefore, avoided here.

### The Linear-Eddy Single Phase Model

In the baseline LEM model (e.g., Kerstein, 1989, 1992; Menon et al., 1993) the exact reaction-diffusion equations are numerically solved using a finite-difference scheme in the local subgrid 1D domain using a grid fine enough to resolve the Kolmogorov and/or the Batchelor microscales. Consequently, the production rate $\dot{\omega}_\alpha$ can be obtained without any modeling. Simultaneous to the deterministic evolution of the reaction-diffusion processes, turbulent convective stirring within the 1D domain is modeled by a stochastic mapping process (Kerstein 1992). This procedure models the effect of turbulent eddies on the scalar fields and is implemented as an instantaneous rearrangement of the scalar fields without changing the magnitudes of the individual fluid elements, consistent with the concept of turbulent stirring.

The implementation of the stirring process requires (randomly) determining the eddy size $l$ from a length scale pdf $f(l)$ in the range $\eta \le l \le l_{LEM}$ where $\eta$ is the Kolmogorov scale and $l_{LEM}$ is the characteristic subgrid length scale which is currently assumed to be the local grid resolution $\Delta$. A key feature of this approach is that this range of scales is determined from inertial range scaling as in 3D turbulence for a given subgrid Reynolds number: $Re_{LEM} = u' l_{LEM}/\nu$ where, $u'$ is obtained from $k_s$. Thus, the range of eddy sizes and the stirring frequency (or event time) incorporates the fact that the small scales are 3D. This feature is one of the major reasons for the past successes of LEM in gas phase diffusion flame studies (Menon and Calhoon, 1996; Calhoon and Menon, 1996, 1997).

### The Linear-Eddy Two-Phase Model

For two-phase flows, the LEM reaction-diffusion equations have been modified to include two new features: (a) the vaporization of the droplets tracked by the Lagrangian method, and (b) the effects of droplets below the cut-off so that the final stages of droplet vaporization and mixing is included. However, some changes are required since droplet vaporization will change the subgrid mass of the gas (primarily the fuel). Thus, in addition to the scalar reaction-diffusion equations, the two-phase mass conservation equations must be solved in the subgrid.

The droplets below the cutoff have been included by assuming that the droplets act as a psuedo-fluid and therefore, the overall effect of the droplets within each LES cell can be modeled as a void fraction. This approach is valid only when the droplets form only a small fraction of the total volume. However, this is an acceptable assumption here since all droplets larger than the cut-off are still tracked using the Lagrangian approach. The present Eulerian two-phase approach is also preferred (in terms of accuracy) when compared to the Lagrangian approach when the droplets are very small and begin to behave more like a continuum fluid.

Mass conservation in both the phases in the LEM is given by: $\rho_g \varphi + \rho_l (1 - \varphi) = \rho_{avg}$, where subscript g represents gas phase, $l$ the liquid phase and $\varphi$ is the volume fraction of the gas phase (1 - void fraction of the liquid ($\lambda$)). The void fraction $\lambda$ or $\varphi$ evolve during the subgrid evolution. Although, the liquid density is a constant, the gas density $\rho_g$ changes and needs to be

determined. The equations in the LEM are:

$$\frac{\partial \rho_g \varphi}{\partial t} = S_L + S_2 \tag{12}$$

$$\frac{\partial (1-\varphi)\rho_l}{\partial t} = S_1 - S_2 \tag{13}$$

Here, the source term $S_1$ is the contribution of the supergrid to the subgrid liquid phase when the droplet size falls below the cutoff. $S_L$ is due to vaporization of the droplets tracked in the supergrid, while $S_2$ represents vaporization of liquid in the subgrid.

The gas phase species equation for any scalar mass fraction ($\Psi$) in the subgrid can be written as

$$\frac{\partial \rho_g \varphi \psi}{\partial t} = D\frac{\partial^2 (\rho_g \varphi \psi)}{\partial s^2} + \dot{\omega}_\psi + S_\psi + S_L \tag{14}$$

Here, "s" indicates the 1D domain of LEM. Also, $S_\psi$ is the source term (only in the fuel species equation) for production due to vaporization of the liquid phase. An equation for temperature must also be solved with the above equations since vaporization requires heat absorption and is followed by a drop in temperature. This is quite similar to the method used in the earlier gas phase studies of heat release effect (Calhoon and Menon, 1997).

Note that, in Equations (12-14) the convective terms are missing. This is consistent with the LEM approach, whereby, the convection of the scalar fields is modeled using the small-scale turbulent stirring and by the splicing process (briefly described below) as noted earlier (Menon et al., 1993a).

### Subgrid implementation of LEM

Since the filtered species $\overline{Y_\alpha}$ is calculated directly by filtering the subgrid $Y_k$ fields, there is no need to solve the LES filtered equations (i.e., Eq. 4). Consequently, use of conventional (gradient diffusion) models is avoided. However, since the $Y_k$ subgrid fields are also influenced by large scale convection (due to the velocity field $\overline{u}_i$ and the subgrid turbulent fluctuation estimated from $k_s$), additional coupling processes are required.

The convection of the scalar fields by the LES field across LES cell faces is modeled by a "splicing" algorithm (Menon et al., 1993; Menon and Calhoon, 1996; Calhoon and Menon, 1996). Details of this process are given in the cited references. Given the initial subgrid scalar fields and void fraction, droplet vaporization, reaction-diffusion, turbulent stirring, and large scale convection processes are implemented as discrete events. The epochs of these processes are determined by their respective time scales. This type of discrete implementation is similar to the fractional step method used to solve the differential equations.

The splicing algorithm transports subgrid fluid elements from one LES cell to another based on the local velocity field. The local velocity consists of the resolved velocity $\overline{u}_i$ plus a fluctuating component (estimated from the subgrid kinetic energy). The splicing events are implemented discretely on the convective time scale. Each splicing event involves (1) the determination of volume transfer between adjacent LES grid cells, (2) the identification of the subgrid elements to be transferred, and (3) the actual transport of the identified fluid elements. The underlying rationale for this procedure has been discussed elsewhere (Calhoon and Menon, 1996). The same algorithm is used here except that now both the scalar fields and the void fraction are spliced at the same time.

An important property of the splicing algorithm is that the species convection is treated as in Lagrangian schemes. Thus, convection is independent of the magnitude or gradient of the species which are transported and depends only on the velocity field. This property allows this algorithm to avoid false diffusion associated with numerical approximation of convective terms in differential equations. By avoiding both numerical and gradient diffusion, the splicing algorithm allows an accurate picture of the small scale effects of molecular diffusion to be captured, including differential diffusion effects.

## RESULTS AND DISCUSSION

The two-phase subgrid model has been implemented into a 3D zero-Mach number code developed earlier (Chakravarthy and Menon, 1997). Briefly, this code solves the LES equations on a non-staggered grid. Time integration is achieved using a two-step semi-implicit fractional step method that is second-order accurate. The spatial difference scheme is fifth-order for the convective terms and fourth-order for the viscous term. The Poisson equation for pressure is solved numerically using a second-order accurate elliptic solver that uses a four-level multigrid scheme to converge the solution. The Lagrangian tracking of the droplets is carried out using a fourth-order Runge-Kutta scheme.

Before simulating reacting flows, an attempt was

made to validate the Lagrangian approach of particle tracking. Although quantitative comparison with earlier studies is difficult due to differences in the set up and/or initial conditions, qualitative comparison can be carried out. For this purpose we simulated the mixing layer studied by Lazaro and Lasheras (1992a,b) and simulated by Martin and Meiburg (1994) using a 2D vortex method. Here, we employed a 3D approach and simulated a temporal mixing layer on a 32x32x32 grid. The particles were injected in every cell of the upper stream with velocities equal to the local cell values. The total number of particles tracked is 13,500. This case is very similar (except for the high resolution both in grid and number of particles) to the direct simulation of Martin and Meiburg (1994). Using the 0.9-0.1 level thickness (Lazaro and Lasheras, 1992b), particle dispersion was computed for a range of Stokes numbers. Here, Stokes number is defined as: $St = (\rho_p d_p^2/18\mu)\Delta U/\delta_\omega$, where $\delta_\omega$ is the vorticity thickness and $\Delta U$ is the velocity difference between the upper and lower stream. Also, the 0.9-0.1 level thickness ($\delta_L$) is the difference between the cross-stream locations where the particle concentrations are 90% and 10% of the reference value, respectively.

Figure 1a shows the dispersion of particles (in terms of the dispersion thickness) with time for a range of Stokes numbers. It can be seen that particles of order $St=1$ exceeds that of droplets with $St<1$ (i.e., smaller droplets). This phenomena was observed earlier in both experimental (Lazaro and Lasheras, 1992b) and numerical (Martin and Meiburg, 1994) studies and was attributed to the increased lateral dispersion of the particles when the aerodynamic response time is of the order of the characteristic flow time. The present result agrees with this result. The increased particle dispersion leads to the formation of streaks for particles for $St=2.5$ as shown in Fig. 1b. These results also agree with earlier observations.

In the following, the discussion focuses primarily on comparing the subgrid model with the conventional model. For these studies, droplets were injected into the core of the mixing layer at time t=0. The mixing layer is initialized by a tangent hyperbolic mean velocity along with the most unstable 2D (of dimensional wavelength $2\pi$) mode and random turbulence (similar to that described in Metcalfe et al., 1987). Results shown here employed a grid resolution of 32x32x32. Grid independence studies were also carried out for some of these cases using a 64x64x64 grid and good agreement was obtained.

The mixing layer is initialized with the oxidizer in both the upper and lower streams at 350 K and the fuel droplets are initially introduced in the mid-plane. A range of droplets from 10-50 micron radius with an initial temperature of 300 K was used for all simulations with the droplet cut-off radius at 5 micron. A total of 2100 droplet groups were tracked (the effect of varying the droplet group has not yet been carried out). For simplicity, the droplet groups were uniformly distributed and the number of droplets in each group is chosen such that the overall mass loading is 0.5 and the corresponding volume loading is 0.0005.

Figure 2a shows the spanwise vorticity contours in the mixing layer at the roll-up stage for a case in which the particles are passively transported upon insertion (i.e., no vaporization included and hence, there is no coupling between the two phases). It can be seen that the shear layer rolls into coherent structures as seen in pure gas phase flows. However, when droplet vaporization is included, as shown in Fig. 2b, the associated heat absorption results in major changes in the shear layer. The formation of the coherent spanwise vortices is inhibited due to vaporization (and mass addition to gas phase). Although the extent of the mixing layer appears to be large, the peak value of the spanwise vorticity is substantially lower for the vaporizing case. Analysis shows that, in the vaporization case, significant 3D vorticity is generated and this plays a major role in the inhibiting the spanwise coherence.

The enhancement of streamwise vorticity can be visualized by comparing Figs. 3a and 3b which show, respectively, the streamwise vorticity for the passive and vaporization cases. The 3D nature of the shear layer has been enhanced in the vaporization case (notice that the same contour interval is employed for direct comparison). Further analysis shows that vaporization causes significant production of the baroclinic torque (the spanwise component of the baroclinic torque, $\nabla\rho X\nabla p/\rho^2$ is shown in Fig. 4a) outside the vortex core. This production plays a major role in redistributing the vorticity in the mixing layer. This can be confirmed by calculating the various terms in the 3D vorticity transport equation. For example, the expansion term $\vec{\omega}(\nabla \bullet \vec{v})$ in vorticity equation is shown in Fig. 4b. Comparison with Fig. 4a indicates that baroclinic term dominates in this case. Interestingly, this behavior is quite similar to the case when heat is released (McMurtry et al., 1989) except that, in the present case, heat is absorbed and the temperature is decreasing.

The droplet distribution for the above two cases is shown in Figs. 5a and 5b, respectively. The Stokes number for all the droplets tracked is in the range of 0.0004-0.01. As expected, the droplets follow the fluid motion and this behavior qualitatively agrees with the results obtained by Ling et al. (1997). Differences exist due to modulation of the vortex structures as a result of

vaporization (as noted above).

LES using the new subgrid model were then compared to identical conventional LES. For these studies, a subgrid resolution that captured the effect of turbulent stirring by the largest small scales (here, for simplicity, a subgrid eddy size 60% of the grid resolution is used), was used to reduce the computational cost. Subgrid resolution was doubled and similar results were obtained indicating that the present tests captures the effect of the largest subgrid scales quite accurately.

The spanwise and streamwise vorticity for the conventional and subgrid approach are shown in Figs. 6a and 6b, respectively, and correspond to Figs. 2b and 3b for the conventional case. The effect of vaporization on shear layer is qualitatively similar in nature but the magnitude is much higher for the subgrid approach. This can be explained by noting that in the LEM approach phase change occurs in the subgrid. Similarity in the droplet distribution is more apparent and can be observed by comparing Figs. 6c and 5b. However, this is not too surprising since the larger droplets are still tracked using the Lagrangian method in both the LES.

Note that, in the subgrid case, if the droplet cut-off is chosen such that no droplet drops below the cut-off, then the void fraction is zero. In this case, the subgrid and the conventional approaches should agree reasonably well. This has been confirmed using infinite kinetics when the vaporized fuel mixes with the oxidizer and reacts. The product mass fraction predicted by the conventional and the Subgrid approaches are compared in Fig. 7a. It can be seen that there is very good agreement thereby confirming the validity of the subgrid approach. The predicted temperature of the gas phase (Fig. 7b) also shows good agreement.

If the cut-off size is large, then it is expected that the conventional LES will be in significant error since it assumes that all droplets below cut-off instantaneously vaporize. However, if the new subgrid approach can deal with this increased cut-off size (by the subgrid void fraction approach) then it will reduce the computational cost of the Lagrangian tracking considerably. To determine this, two cut-off sizes of 10 and 20 microns were used in otherwise identical simulations. Since the droplet distribution is lost once the drops are in the subgrid, it is assumed that all the droplets are at the average diameter between the cut-off and zero. This is not an accurate assumption and in the future, droplet distribution information will be carried to the subgrid. Another source of error is that, currently, the liquid void fraction is passively transported across LES cells based on the volume transfer of the gas phase. However, the liquid phase transport should be based on the liquid volume transfer from the LES cell. A method to deal with this transport has been developed and will be used in future studies.

The product mass fraction obtained by the two different LES methods is compared in Fig. 8 for the various cut-off sizes. The results predicted by the conventional LES are in gross error for cut-off radius of 10 and 20 micron. However, the present methodology captures most of the trends and magnitudes. Ideally, the subgrid model should predict identical results for a range of cut-off sizes. The observed differences in the magnitude and the spread are due to the lower vaporization rates in the core region. Analysis shows that this is primarily due to above noted problem with the LES transport of the liquid phase. It is expected that the correction developed for this will result in more consistent predictions.

Finite rate cases for three different Damkohler numbers (Da) were also simulated. The product mass fractions for different Da are shown in Fig. 9a and the temperatures are compared in Fig. 9b. When the chemical time scale decreases (Da increases), the product mass fraction increases in agreement with earlier results and physics. Due to finite-rate effects, there is a considerable amount of unreacted fuel in the gaseous form. In addition to the droplet temperature and the surrounding oxidizer concentration, the amount of fuel present in the gaseous form dictates the liquid to gaseous fuel phase change. Thus, the vaporization rate is coupled to the rate of chemical kinetics, heat release and the other processes such as convection. The demonstration that the present method can capture Da-effects needs to be reevaluated in the presence of heat release. Furthermore, since the present method can deal with differential diffusion, Lewis number effects can also be captured. This will be demonstrated in the near future.

## CONCLUSIONS

In this study, an earlier developed gas phase subgrid combustion model has been extended for two-phase flows. This approach includes a more fundamental treatment of the effects of the final stages of droplet vaporization, molecular diffusion, chemical reactions and small scale turbulent stirring than other LES closure techniques. As a result, Reynolds, Lewis and Damkohler number effects are explicitly included. This model has been implemented within an Eulerian-Lagrangian two phase large-eddy simulation (LES) formulation. In this approach, the liquid droplets are tracked using the Lagrangian approach up to a pre-

specified cut-off size. However, the vaporization of the Lagrangian droplets and the evaporation and mixing of the droplets smaller than the cut-off size are modeled within the subgrid using an Eulerian two-phase model that is an extension of the earlier gas-phase subgrid model. The issues (both resolved and unresolved) related to the implementation of this subgrid model within the LES are discussed in this paper.

The present results on the increased dispersion of non-vaporizing droplets at intermediate sizes in forced mixing layers agrees well with trends seen in earlier experimental and numerical studies. When vaporization was included, modifications of the vortex structure was found to be due to the production of baroclinic torque. This result is quite similar to the heat release effect seen earlier. The effect of varying the Damkohler number was also captured correctly. Finally, it has been shown that when the droplet cut-off size is increased, the conventional method gives erroneous results while the current methodology captures most of the trends within the limitation of the current implementation.

## ACKNOWLEDGMENTS

This work was supported in part by the Army Research Office Multidisciplinary University Research Initiative grant DAAH04-96-1-0008 and by the Air Force Office of Scientific Research Focused Research Initiative contract F49620-95-C-0080 monitored by General Electric Aircraft Engine Company, Cincinnati, Ohio. Computations were carried out under the DoD HPC Grand Challenge Project at ARC, Huntsville.

## REFERENCES

Calhoon, W.H. and Menon, S. (1996) "Subgrid Modeling for Reacting Large-Eddy Simulations," AIAA 96-0516, 34th AIAA Aerospace Sciences Meeting.

Calhoon, W.H. and Menon, S. (1997) "Linear-Eddy Subgrid Model for Reacting Large-Eddy Simulations: Heat Release Effects," AIAA 97-0368, 35th AIAA Aerospace Sciences Meeting.

Faeth, G. M. (1983) "Evaporation and Combustion of Sprays," Progress in Energy and Combustion Science, Vol. 9, pp. 1-76.

Kerstein, A. R. (1989) "Linear-Eddy Model of Turbulent Transport II. Application to Shear Layer Mixing," Combustion and Flame, Vol. 75, pp. 397-413.

Kerstein, A. R. (1992) "Linear-Eddy Model of Turbulent Transport 4. Structure of Diffusion-Flames," Comb. Sci. and Tech., Vol. 81, pp.75-96.

Ling, W., Chung, J. N., Troutt, T. R., and Crowe, C. T. (1997) "Numerical Simulation of Particle Dispersion in a Three-dimensional Temporal Mixing Layer," 1997 ASME Fluids Engineering Division Summer Meeting, Vancouver.

Lazaro, B. J., and Lasheras, J. C. (1992a) "Particle Dispersion in the Developing Free Shear Layer," J. Fluid Mech., Vol. 235, pp. 143-178.

Lazaro, B. J., and Lasheras, J. C. (1992b) "Particle Dispersion in the Developing Free Shear Layer," J. Fluid Mech., Vol. 235, pp. 179-221.

Martin, J. E. and Meiburg, E. (1994) "The Accumulation and Dispersion of Heavy Particles in Forced Two-dimensional Mixing Layers. I. The Fundamental and Subharmonic Cases," Phys. Fluids, Vol. 6 (3), pp. 1116-1132.

McMurtry, P. A., Riley, J. J., and Metcalfe, R. W. (1989) "Effects of Heat Release on the Large-scale Structure in Turbulent Mixing Layers," Journal of Fluid Mech., Vol. 199, pp. 297-332.

Menon, S., McMurtry, P., and Kerstein, A.R. (1993a) "A Linear Eddy Mixing Model for LES of Turbulent Combustion," in Large-Eddy Simulations of Complex Engineering and Geophysical Flows, (B. Galperin and S.A. Orszag, Eds.), Cambridge Univ. Press, pp. 278-315.

Menon, S. and Chakravarthy, V. K. (1996) "Large-Eddy Simulations of Premixed Flames in Couette Flow," AIAA 96-3077, 32nd AIAA/ASME/SAE/-ASEE Joint Prop. Conference.

Menon, S. and Kim, W.-W. (1996) "High Reynolds Number Flow Simulations using the Localized Dynamic Subgrid-Scale Model," AIAA 96-0425, 34th AIAA Aerospace Sciences Meeting.

Menon, S. and Calhoon, W. (1996) "Subgrid Mixing and Molecular Transport Modeling for Large-Eddy Simulations of Turbulent Reacting Flows," Symp. (International) on Combustion, 26.

Metcalfe, R. W., Orszag, S. A., Brachet, M. E., Menon, S., and Riley, J. J. (1987) "Secondary Instability of a Temporally Growing Mixing Layer," J. Fluid Mech., Vol. 184, pp. 207-243.

Mostafa, A. A. and Mongia, H. C. (1983) "On the Modeling of Turbulent Evaporating Sprays: Eulerian versus Lagrangian Approach," Int. J. of Heat Mass Transfer, Vol. 30, pp. 2583-2593.

Oefelein, J. C. and Yang, V. (1996) "Analysis of Transcritical Spray Phenomena in Turbulent Mixing Layers," AIAA 96-0085, 34th AIAA Aerospace Sciences Meeting, Reno, NV, Jan. 15-18.

Poinsot, T. (1996) "Using Direct Numerical Simulations to Understand Premixed Turbulent Combustion," 26th Symp. (Intn.) on Combustion, pp. 219-232.

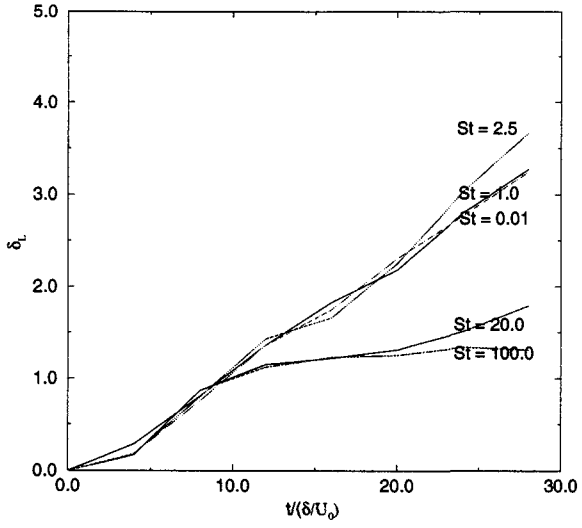


Figure 1a) Evolution of the 0.9-0.1 particle concentration level thickness for various St.

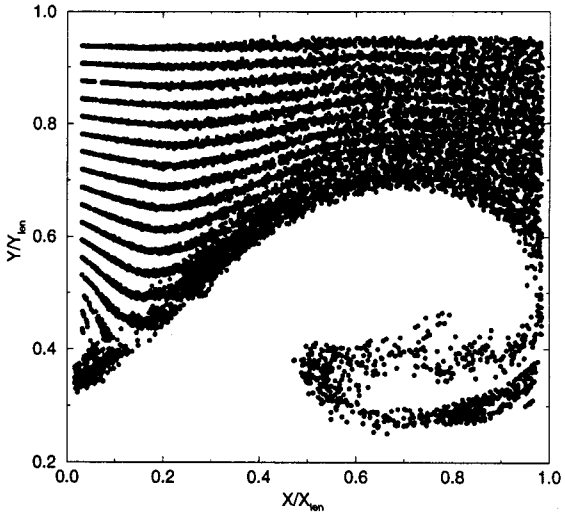


Figure 1b) Projection of the droplet distribution in the X-Y for particles of St. = 2.5 at t=28.

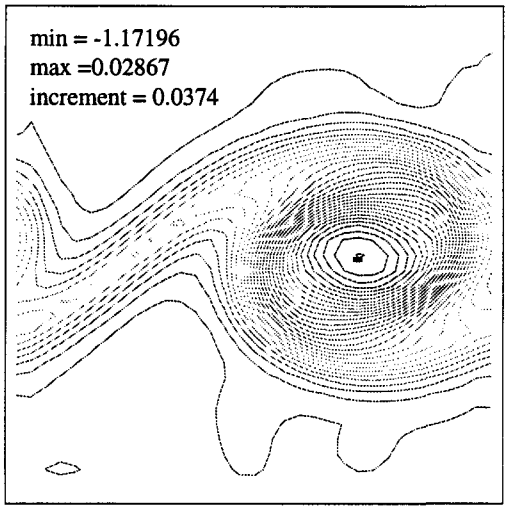


Figure 2a) Spanwise vorticity in the mixing layer without coupling from liquid phase. Nondimensionalized by $U_0/L_0$

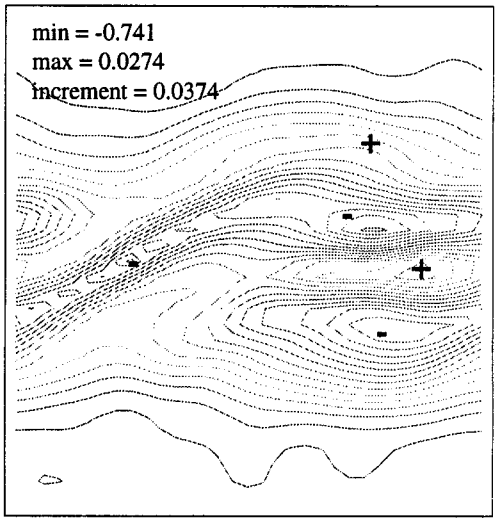


Figure 2b) Spanwise vorticity in the mixing layer with coupling from liquid phase (Conventional LES).

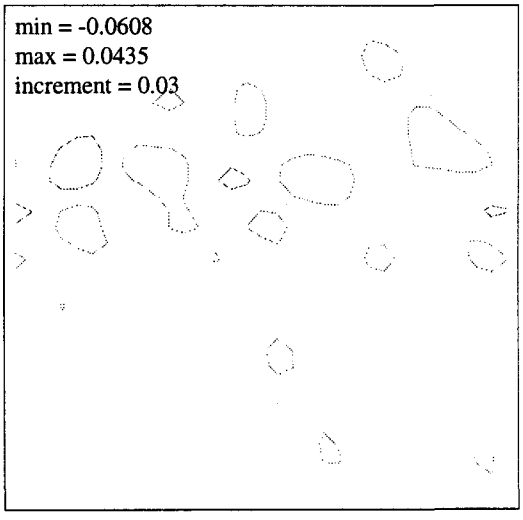


Figure 3a) Streamwise vorticity in the mixing layer without coupling from liquid phase.

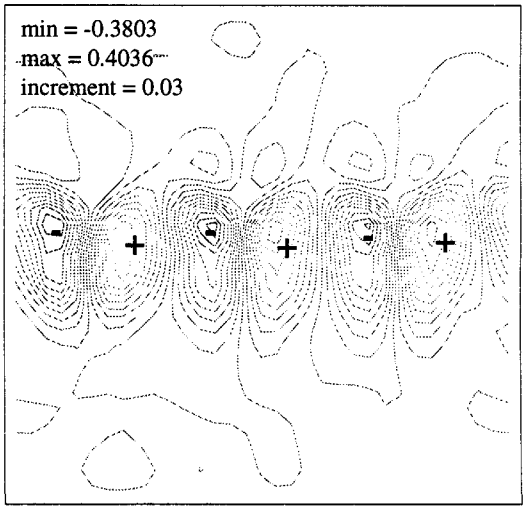


Figure 3b) Streamwise vorticity in the mixing layer with coupling from liquid phase (Conventional LES).

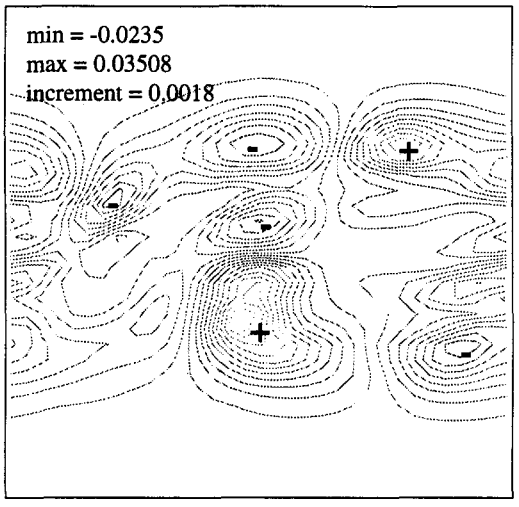


Figure 4a) Instantaneous value of spanwise component of the baroclinic term in vorticity equation in mid-span plane.

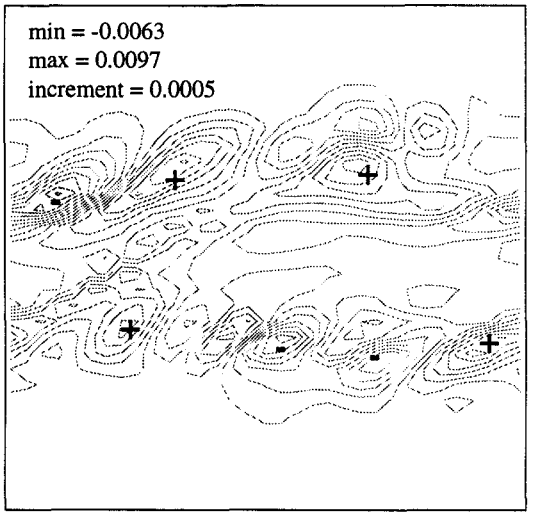


Figure 4b) Instantaneous value of spanwise component of the expansion term in vorticity equation in mid-span plane.

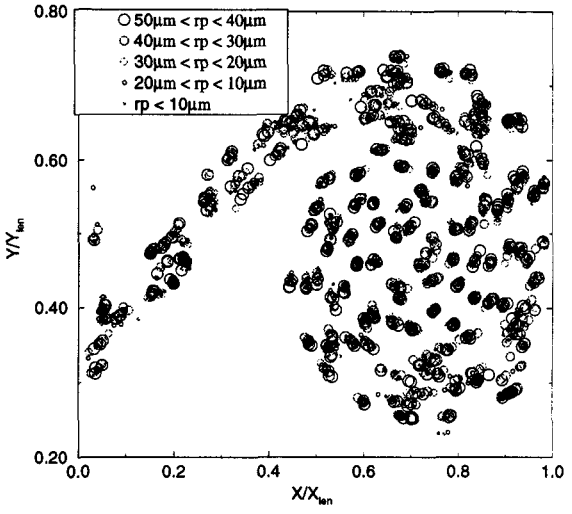


Figure 5a) Projection of the droplet distribution in the X-Y plane without coupling from liquid phase.

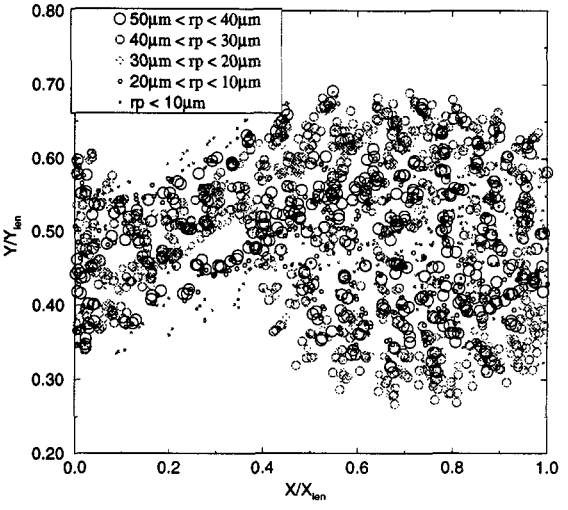


Figure 5b) Projection of the droplet distribution in the X-Y plane with coupling from liquid phase (Conventional LES).

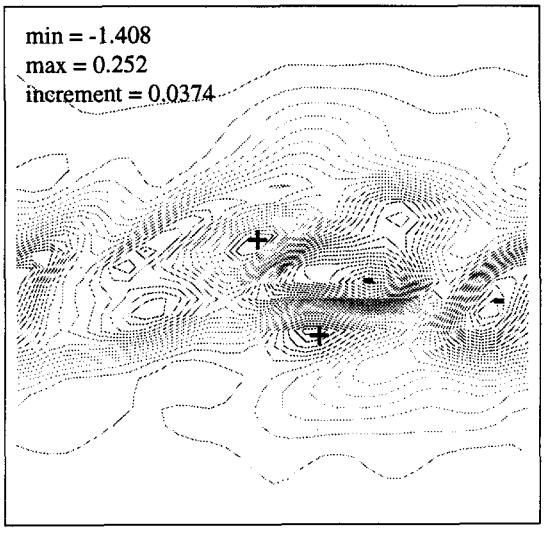


Figure 6a) Spanwise vorticity in the mixing layer with coupling from liquid phase (LES/LEM).

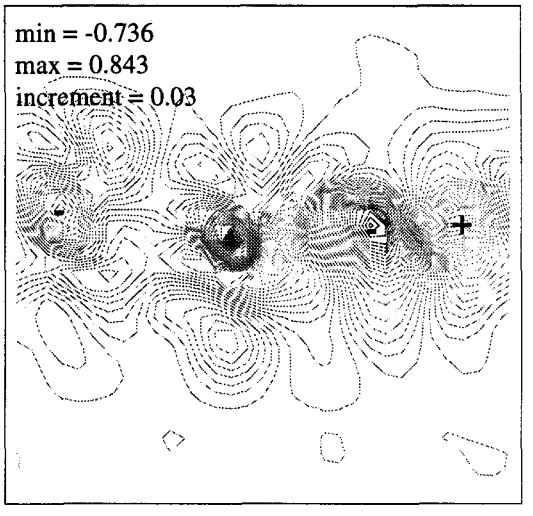


Figure 6b) Streamwise vorticity in the mixing layer with coupling from liquid phase (LES/LEM).

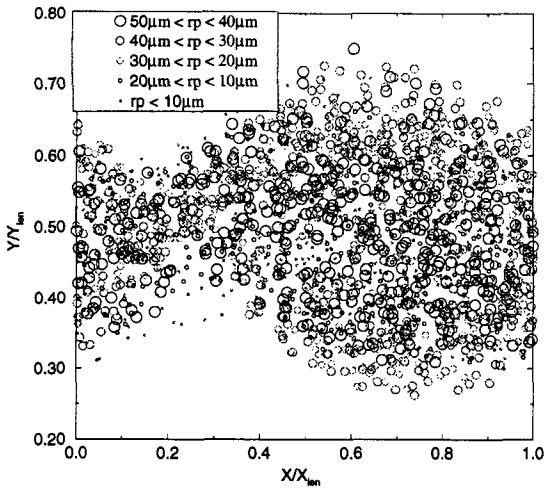


Figure 6c) Projection of the droplet distribution in the X-Y plane with coupling from liquid phase (LES/LEM).

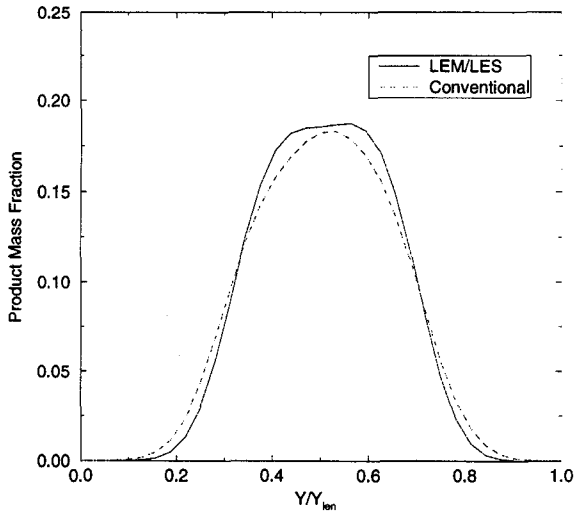


Figure 7a) Variation of X-Z plane averaged product mass fraction across the mixing layer for infinite rate.

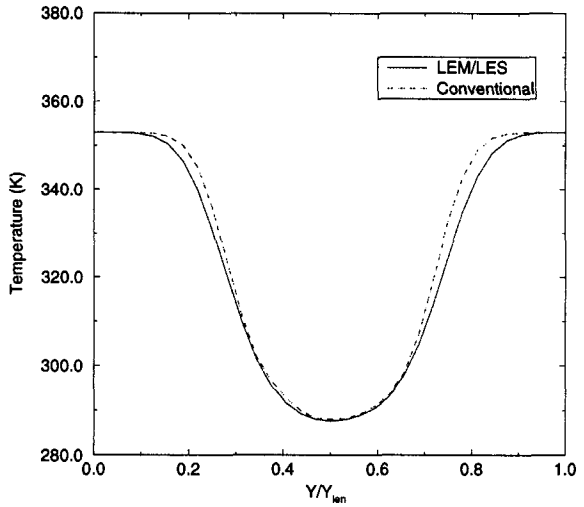


Figure 7b) Variation of X-Z plane averaged temperature across the mixing layer for infinite rate.

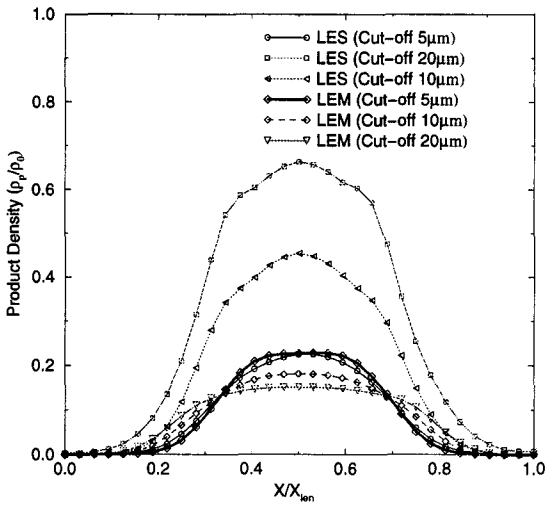


Figure 8) Variation of X-Z plane averaged product density across the mixing layer for different cut-offs.

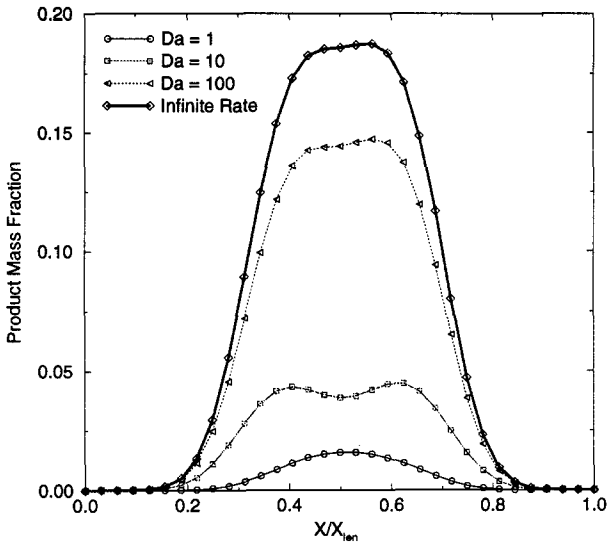


Figure 9a) Variation of X-Z plane averaged product mass fraction across the mixing layer for different Damkohler numbers.

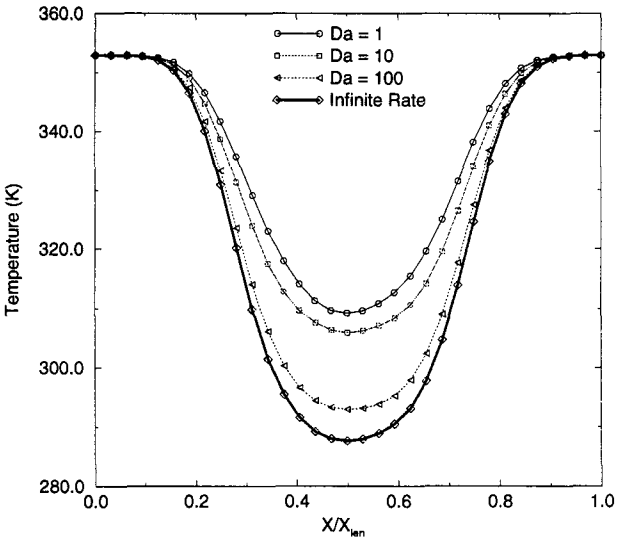


Figure 9b) Variation of X-Z plane averaged temperature across the mixing layer for different Damkohler numbers.